International Journal of Thermofluid Science and Technology (2023)
Volume 10, Issue 2, Paper No. 100204
https://doi.org/10.36963/IJTST.2023100204

Research Article

Conjugate heat transfer in an annulus with heated longitudinal and transversal fins

Hassen Haithem[1], SofianeTouahri[1] and Toufik Boufendi[1,2*]

[1]*Energy Physics Laboratory, Physics Department, University of Constantine 1, 25000, Algeria*
[2]*University August 20, 1955, Skikda, Algeria*

ARTICLE INFO

Received: 18 Nov. 2022;
Received in revised form:
06 Jun. 2023;
Accepted: 13 Jun. 2023;
Published online:
20 Jun. 2023

Keywords:
Conjugate heat transfer
Longitudinal fins
Transversal fins
Mixed convection
Numerical simulation

ABSTRACT

In this work, we numerically study the three-dimensional conjugate mixed convection heat transfer in a horizontal annulus equipped by longitudinal and transversal fins attached on its internal surface of outer cylinder. The external pipe and fins are heated by an electrical current passing through their small thickness while the inner pipe is kept adiabatic. We investigate the effects of adding longitudinal and transversal fins on the fluid dynamic and the heat transfer performances. The number of longitudinal fins varies from two to eight fins while the number of transvers ones is equal to four. The convection in the fluid domain is conjugated to thermal conduction in the pipes and fins solid thickness. The physical properties of the fluid are thermal dependent and the heat losses from the external pipe surface to the surrounding environment are taken account. The model equations of continuity, momenta and energy are numerically solved by the finite volume method with a second order spatiotemporal discretization. The Prandtl, the Reynolds and the Grashof numbers are fixed at 8.082, 399.02 and 12801 respectively. The obtained results showed that the axial Nusselt number increases with the increasing of number of fins. Moreover, the longitudinal fins configuration showed a more significant improvement in heat transfer than that of the transverse fins.

1. Introduction

The problem of using fins to increase the exchange surfaces between the fluids and the walls of the ducts is often studied in many engineering sectors in order to improve heat transfer. In this context, the geometric shape and orientation of the fins studied are very important factors for increasing the efficiency of heat transfer. Much research, both experimental and numerical, has been carried out for different types of finned ducts. Patankar et al. [1] presented an analytical model for fully developed turbulent air flow in internally finned tubes and annuli. In their study, the longitudinal attached fins in the inner wall were considered. The thermal boundary conditions were a constant heat flux at the inner surface; the obtained results are presented as determining the Nusselt numbers and coefficients of charge loss. Agrawal et al. [2], numerically studied the effect of varying the geometric parameters and the Reynolds number on the pressure drop and

*Corresponding e-mail: t.boufendi@univ-skikda.dz (Toufik Boufendi)

Nomenclature

D_{1i}	internal diameter of inner pipe, m	t^*	non-dimensional time, $V_0\, t/D_h$
D_{1o}	external diameter of inner pipe, m	T	temperature, K
D_{2i}	internal diameter of outer pipe, m	T^*	non-dimensional temperature, $(T-T_0)/(G\ D_h^2/K_s)$
D_{2o}	external diameter of outer pipe, m	V_0	axial velocity at the entrance, m/s
D_h	hydraulic diameter $=D_{2i}$-D_{1o} ,m	V^*	non-dimensional velocity, V^*/V_0
L	annulus length, m	z^*	non-dimensional axial coordinate, z/D_h
H	fin height, m	*Greek symbols*	
g	gravitational acceleration, =9.81m/s^2	α	thermal diffusivity, m^2/s
G	volumetric heat generation, w/m^3	β	thermal expansion coefficient, (1/K)
Gr^*	modified Grashof number, $(g\,\beta\,G\ D_h^5/K_s\,\nu^2)$	ε	emissivity coefficient
h_r	radiative heat transfer coefficient, w/m^2 K	θ	angular coordinate, rad
h_c	convective heat transfer coefficient, w/m^2 K	μ	dynamic viscosity, kg /m s
K^*	thermal conductivity, K/K_0	ν	cinematic viscosity, m²/s
Nu	Nusselt number	τ	the viscous stress tensor, kg/m^2 s
P	pressure, kg/m s^2	τ^*	non-dimensional stress, $\tau/(\mu_0 V_0/D_i)$
P^*	non-dimensional pressure, $(P-P_0)/\rho_0 V_0^2$	*Subscripts*	
Pr	Prandtl number, ν/α	i	internal
r	radial coordinate, m	o	external
Re	Reynolds number, $V_0\, D_h/\nu_0$	*Superscripts*	
t	time, s	*	dimensionless

the heat transfer. This study was conducted for the case of longitudinal fins attached to the inside of an annulus. In the numerical work of Farinas et al. [3], the authors studied the laminar mixed convection in an annulus with three different configurations of fins: two, four and sixteen fins. The inner wall is heatedt while the outer wall is cooled. The Grashof number varied from 10^2 to 10^4 and the conservation equations are solved by the finite difference method. The results are presented for the air with Rayleigh numbers varying from10^3 to 10^6 for different configurations of fins (fine rounded or divergent) with different lengths (L=0.25, 0.5 and 0.75). The results are presented as isotherms graphs, velocity fields and Nusselt numbers variation.

The heat transfer is enhanced to a rounded configuration of the fins. Khemici et al. [4] and Touahri et al. [5] studied numerically the conjugate heat transfer by mixed convection in horizontal pipe without fins. In [6], Touahri et al. studied the same problem, but in this case the horizontal pipes are equipped by longitudinal and transversal attached fins on its internal wall. The mixed convection is there by conjugate with thermal conduction in the pipe and fins walls. The physical properties of the fluid are thermo-dependent and the heat losses with the external environment are considered. The obtained results show that the use of longitudinal and transverse fins increases the Nusselt number very significantly. In the numerical work of Benhacine et al. [7], the authors studied forced and mixed convection without and with a magnetic field. three objectives are achieved: The first objective is to clarify the effects of annular spaces on vortex breakdown (appearance and suppression) in which three annular spaces are compared. The second objective is to identify the intensity of the magnetic field corresponding to the elimination of the vortex bubble. The third objective is to specify the role of the temperature gradient on the appearance of the bifurcation in the form of fluid sheets. Finally,

it is a question of specifying the intensity of the magnetic field corresponding to the withdrawal of the fluid layers. The stability limits corresponding to the domain where stratification does not occur are presented. The flow and heat transfer characteristics of a tube with an integrated internal longitudinal fin were studied by experiment and numerical simulation by Liu et al. [8], the effects of inscribed circle diameter and fin included angle on the thermal performance were investigated by numerical simulation. The obtained numerical results were in good agreement with the experimental data. A similar study was also treated numerically and experimentally by Yuzhu et al. [9]. The heat transfer by natural convection of a laminar flow of water between two concentric cylinders is studied numerically by Gourari et al. [10], the inner cylinder generates a constant heat source while the outer cylinder is cold, the upper and lower walls are thermally insulated, the angles of inclination studied are: 0°, 45°, 90°. The results obtained showed that the mean Nusselt number increases with increasing Rayleigh numbers and the best heat transfer is obtained for the 90° tilt angle. Solving a coupled system of equations composed of the Navier-Stokes, conservation of electric charge and Poisson equations was the objectif of the work studied by Elkhazen et al. [11]. All of these coupled equations are solved for the first time in this work using elliptical-cylindrical coordinates.

On the other hand, the use of nanofluids significantly improves the heat transfer in the annulus with or without fins. In the review papers of Hussein [12, 13], Hussein et al. [14, 15], Mahian et al. [16, 17], Li et al. [18], Ghachem et al. [19] and Kamel et al. [20], several applications of nanotechnology are well detailed.

In their work, Benkhedda et al. [21] have numerically studied laminar mixed convection in horizontal annulus filled with a TiO_2/water nanofluid and Ag-TiO_2/water hybrid nanofluid has. The outer cylinder is uniformly heated, the inner cylinder is adiabatic. The nanoparticles volume fraction is between 0 and 8% and Grashof numbers between 10^5 and 10^6. The results shows that the local and average Nusselt numbers, and the bulk temperature increase with the increasing of the volume fraction and the Grashof number also the heat transfer is very enhancement when using a Ag-TiO_2/water hybrid nanofluid compared to the similar TiO_2/water nanofluid.

In their numerical work, Tayebi et Chamkha have studied free convection enhancement of a hybrid nanofluid in eccentric horizontal cylindrical annulus [22] and in an annulus between horizontal confocal elliptical cylinders [23]. The obtained results show that the employing a hybrid mixture delivers an excellent thermal and dynamic performance compared to the similar traditional nanofluid. Similar work on natural convection is also carried out by Tayebi et al. [24–26]. On their part, Al-Rashed et al. [27], numerically treated convective heat transfer and entropy generation in a 3D closed cavity,, equipped with adiabatic-driven baffle and filled with CNT-water nanofluid for a range of Rayleigh numbers from 10^3 to 10^5 and a range of CNT concentrations from 0 to 15%. The use of water-based CNT nanoliquids in natural convection is also investigated by Tayebi et al. [28] under magnetic field within a concentric circular ring between a heat-generating conductive inner cylinder and an isothermal cold outer cylinder filled with an NTC water-based nanoliquid. The results of this study lie the role of the control parameters considered with regard to the hydrothermal characteristics and the rate of heat exchange within the annular space.

In the present work, we have studied numerically the heat transfer by mixed convection in annulus between two concentric cylinders. Longitudinal and transversal fins are attached in the inner wall of the outer cylinder. The mixed convection is conjugated with the thermal conduction in the pipes and fins walls. The physical properties of the fluid are thermo-dependent and heat losses to the outside environment are taken into account while the inner cylinder is adiabatic at its inner wall. The objective of our work is to study the improvement of heat transfer in the annulus using 8 longitudinal fins in the first case and 4 transversal fins in the second case.

2. Geometry and mathematical model

To assure continuity in the research work, the geometry and the nature of the pipes are similar to those considered in the numerical studies conducted in refs. [4–6]. Fig. 1 illustrates the geometry of the problem studied. Two long horizontal concentric cylinders having a length L=1m, the inner tube with an internal diameter D_{1i}=0.46 cm and an outer diameter D_{1o}=0.5 cm, while the outer tube with an internal diameter D_{2i}=0.96 cm and an outer diameter D_{2o}=1 cm.

In first case, longitudinal fins with a height H=0.12 cm (25% of the hydraulic diameter) are attached to the inner wall of the outer cylinder, The studied number of longitudinal fins varies from two to eight ones. For the cas of eight fins, these latters are placed at: ($\theta=0$), ($\theta=\pi/4$), ($\theta=\pi/2$), ($\theta=3\pi/4$), ($\theta=\pi$), ($\theta=5\pi/4$), ($\theta=3\pi/2$) and ($\theta=7\pi/4$).

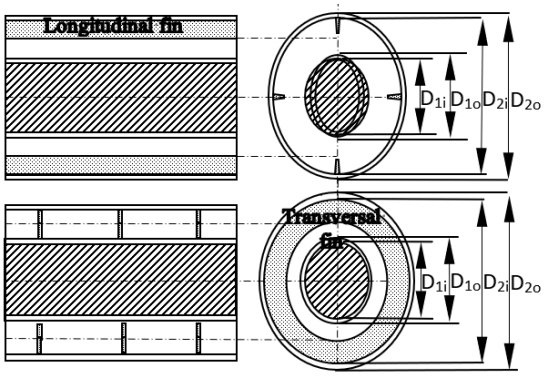

Fig. 1. Geometry of the problem

While in the second case, four transversal fins are attached on the same wall at: z^*=19.701, z^*=63.179, z^*=106.658 and z^*=171.875. The pipes and fins are made of Inconel having a thermal conductivity K_s= 20 W $m^{-1}K^{-1}$. An electric current passing along the external pipe (in the solid thickness) produced a heat generation by Joulean effect. This heat is transferred to distilled water flow in the annulus, while the inner cylinder is adiabatic. At the entrance, the flow has an axial meanvelocity equal to 9.88 10^{-2}m/s and a constant temperature of 15 °C. The density is a linear function of temperature and the Boussinesq approximation is adopted. The physical principles involved in this problem are well modeled by the following non dimensional conservation partial differential equations with their initial and boundary conditions.

The Reynolds number is equal to 399.02 and the Prandtl number is equal to 8.082. The non-dimensional fluid viscosity and thermal conductivity variation with temperature are represented by the functions $\mu^*(T^*)$ and $k^*(T^*)$ obtained by smooth fittings of the tabulated values cited by Baehr and Stephan [29].

2.1 Modelling equations

The physical phenomenon of the conjugate heat transfer, result of the mixed convection in the fluid flow combined with heat conduction in the solid wall and the fins, are modelled by the dimensionless conservations equations with appropriate boundary conditions as follows:

(1) Mass conservation equation

$$\frac{1}{r^*}\frac{\partial}{\partial r^*}\left(r^* V_r^*\right)+\frac{1}{r^*}\frac{\partial V_\theta^*}{\partial \theta}+\frac{\partial V_z^*}{\partial z^*}=0 \tag{1}$$

(2) Radial momentum conservation equation

$$\frac{\partial V_r^*}{\partial t^*}+\frac{1}{r^*}\frac{\partial}{\partial r^*}\left(r^* V_r^* V_r^*\right)+\frac{1}{r^*}\frac{\partial}{\partial \theta}\left(V_\theta^* V_r^*\right)+\frac{\partial}{\partial z^*}\left(V_z^* V_r^*\right)-\frac{V_\theta^{*2}}{r^*}=-\frac{\partial P^*}{\partial r^*}+\frac{Gr_0^*}{Re_0^2}\cos\theta\, T^*+\frac{1}{Re_0}\left[\frac{1}{r^*}\frac{\partial}{\partial r^*}\left(r^*\tau_{rr}^*\right)+\frac{1}{r^*}\frac{\partial}{\partial \theta}\left(\tau_{r\theta}^*\right)-\frac{\tau_{\theta\theta}^*}{r^*}+\frac{\partial}{\partial z^*}\left(\tau_{rz}^*\right)\right] \tag{2}$$

(3) Angular momentum conservation equation

$$\frac{\partial V_\theta^*}{\partial t^*}+\frac{1}{r^*}\frac{\partial}{\partial r^*}\left(r^* V_r^* V_\theta^*\right)+\frac{1}{r^*}\frac{\partial}{\partial \theta}\left(V_\theta^* V_\theta^*\right)+\frac{\partial}{\partial z^*}\left(V_z^* V_\theta^*\right)+\frac{V_r^* V_\theta^*}{r^*}=-\frac{1}{r^*}\frac{\partial P^*}{\partial \theta}-\frac{Gr_0^*}{Re_0^2}\sin\theta\, T^*+\frac{1}{Re_0}\left[\frac{1}{r^{*2}}\frac{\partial}{\partial r^*}\left(r^{*2}\tau_{\theta r}^*\right)+\frac{1}{r^*}\frac{\partial}{\partial \theta}\left(\tau_{\theta\theta}^*\right)+\frac{\partial}{\partial z^*}\left(\tau_{\theta z}^*\right)\right] \tag{3}$$

(4) Axial momentum conservation equation

$$\frac{\partial V_z^*}{\partial t^*}+\frac{1}{r^*}\frac{\partial}{\partial r^*}\left(r^* V_r^* V_z^*\right)+\frac{1}{r^*}\frac{\partial}{\partial \theta}\left(V_\theta^* V_z^*\right)+\frac{\partial}{\partial z^*}\left(V_z^* V_z^*\right)=-\frac{\partial P^*}{\partial z^*}+\frac{1}{Re_0}\left[\frac{1}{r^*}\frac{\partial}{\partial r^*}\left(r^*\tau_{rz}^*\right)+\frac{1}{r^*}\frac{\partial}{\partial \theta}\left(\tau_{\theta z}^*\right)+\frac{\partial}{\partial z^*}\left(\tau_{zz}^*\right)\right] \tag{4}$$

* Energy conservation equation

$$\frac{\partial T^*}{\partial t^*}+\frac{1}{r^*}\frac{\partial}{\partial r^*}\left(r^* V_r^* T^*\right)+\frac{1}{r^*}\frac{\partial}{\partial \theta}\left(V_\theta^* T^*\right)+\frac{\partial}{\partial z^*}\left(V_z^* T^*\right)= \quad (5)$$
$$G^*-\frac{1}{Re_0 Pr_0}\left[\frac{1}{r^*}\frac{\partial}{\partial r^*}\left(r^* q_r^*\right)+\frac{1}{r^*}\frac{\partial}{\partial \theta}\left(q_\theta^*\right)+\frac{\partial}{\partial z^*}\left(q_z^*\right)\right]$$

The viscous stress tensor components are:

$$\tau_{rr}^*=2\mu^*\frac{\partial V_r^*}{\partial r^*},\quad \tau_{r\theta}^*=\tau_{\theta r}^*=\mu^*\left[r^*\frac{\partial}{\partial r^*}\left(\frac{V_\theta^*}{r^*}\right)+\frac{1}{r^*}\frac{\partial V_r^*}{\partial \theta}\right]$$
$$\tau_{\theta\theta}^*=2\mu^*\left[\frac{1}{r^*}\frac{\partial V_\theta^*}{\partial \theta}+\frac{V_r^*}{r^*}\right],\quad \tau_{\theta z}^*=\tau_{z\theta}^*=\mu^*\left[\frac{\partial V_\theta^*}{\partial z^*}+\frac{1}{r^*}\frac{\partial V_z^*}{\partial \theta}\right] \quad (6)$$
$$\tau_{zz}^*=2\mu^*\frac{\partial V_z^*}{\partial z^*},\quad \tau_{zr}^*=\tau_{rz}^*=\mu^*\left[\frac{\partial V_z^*}{\partial r^*}+\frac{1}{r^*}\frac{\partial V_r^*}{\partial z^*}\right]$$

The heat fluxes are:

$$q_r^*=-K^*\frac{\partial T^*}{\partial r^*},\quad q_\theta^*=-\frac{K^*}{r^*}\frac{\partial T^*}{\partial \theta^*},\quad q_Z^*=-K^*\frac{\partial T^*}{\partial z^*} \quad (7)$$

2.2 The boundary conditions

(1) At the annulus entrance: $z^*=0$

In the fluid domain: $V_r^*=V_\theta^*=T^*=0, V_z^*=1$ (8)

In the solid domain: $V_r^*=V_\theta^*=V_z^*=T^*=0$ (9)

(2) At the annulus exit:$z^*=217.39$

In the fluid domain:

$$\frac{\partial V_r^*}{\partial z^*}=\frac{\partial V_\theta^*}{\partial z^*}=\frac{\partial V_z^*}{\partial z^*}=\frac{\partial}{\partial z^*}\left(K^*\frac{\partial T^*}{\partial z^*}\right)=0 \quad (10)$$

In the solid domain:

$$V_r^*=V_\theta^*=V_z^*=\frac{\partial}{\partial z^*}\left(K^*\frac{\partial T^*}{\partial z^*}\right)=0 \quad (11)$$

(3) At the inside wall of internal pipe: $r^*=0.5$

$$V_r^*=V_\theta^*=V_z^*=0 \quad et \quad \frac{\partial T^*}{\partial r^*}=0 \quad (12)$$

(4) At the outer wall of external pipe: $r^*=1.087$

$$\begin{cases} V_r^*=V_\theta^*=V_z^*=0 \\ -K^*\dfrac{\partial T^*}{\partial r^*}=\dfrac{(h_r+h_c)D_i}{K_0}T^* \end{cases} \quad (13)$$

$$h_r=\varepsilon\sigma\left(T^2+T_\infty^2\right)\left(T+T_\infty\right) \quad (14)$$

The emissivity of the outer wall ε is arbitrarily chosen to 0.9 while h_c is derived from the correlation of Churchill and Chu [30].

$$Nu=\left[h_c D_i/K_{air}\right]=\left[0.6+\frac{0.387\,Ra^{1/6}}{\left(1+(0.559/Pr_{air})^{9/16}\right)^{8/27}}\right]^2 \quad (15)$$

2.3 Nusselt number

At the pipe wall interface ($r^*=r_{2i}^*=1.044$) the local Nusselt number is defined as:

$$Nu(\theta,z^*)=\frac{h(\theta,z^*)D_i}{K_0}=\left[\frac{\left(K^*\partial T^*/\partial r^*\right)\big|_{r^*=r_{2i}^*}}{T^*(0.5,\theta,z^*)-T_m^*(z^*)}\right] \quad (16)$$

At the longitudinal fins wall interface ($\theta=\theta_{fin}$), the local Nusselt number is defined as:

$$Nu(r^*,z^*)=\frac{h(r^*,z^*)D_h}{K_0}=\left[\frac{\left(K^*/r^*\right)\left(\partial T^*/\partial \theta\right)\big|_{\theta=\theta_{fin}}}{T^*(r^*,\theta_{fin},z^*)-T_m^*(z^*)}\right] \quad (17)$$

At the transversal fins wall interface ($z=z_{fin}$), the local Nusselt number is defined as:

$$Nu(r^*,\theta)=\frac{h(r^*,\theta)D_h}{K_0}=\left[\frac{\left(K^*\right)\left(\partial T^*/\partial z\right)\big|_{z=z_{fin}}}{T^*(r^*,\theta,z^*_{ailette})-T_m^*(z^*)}\right] \quad (18)$$

2. Numerical resolution

This set of coupled non-linear differential equations with boundary conditions was discretized by the finite volume method, well described by Patankar [31]. The using of this method involves the discretization of the physical domain into a discrete domain constituted of finite volumes where the modelling equations are discretized in a typical volume. For this we use a Fortran source code based on the SIMPLER algorithm [31] which is used to treat the pressure-velocity coupling and to obtain the iterative solution of the discretized model equations involving the use of the tri-diagonal matrix algorithm (TDMA).

The mesh used contains 52×88×162 points in the radial, azimuthal and axial directions successively and the temporal discretization is realised with a truncation error of $(\Delta t^*)^2$ order and the considered time step is $\Delta t^* = 5 \cdot 10^{-4}$. The steady state is controlled by the satisfaction of the global mass and energy balances as well as the leveling off of the time evolution of the hydrodynamic and thermal fields.

In fig. 2 we illustrate the axial evolution of the circumferentially averaged Nusselt number. It is seen that there is good agreement between our results and those of Carlo and Guidice. [32] who studied numerically the conjugate mixed convection heat transfer in annulus with the controlling parameters of the problem: Re=1,000, Pr=0.7, Gr=10^6, and R_2/R_1=1.

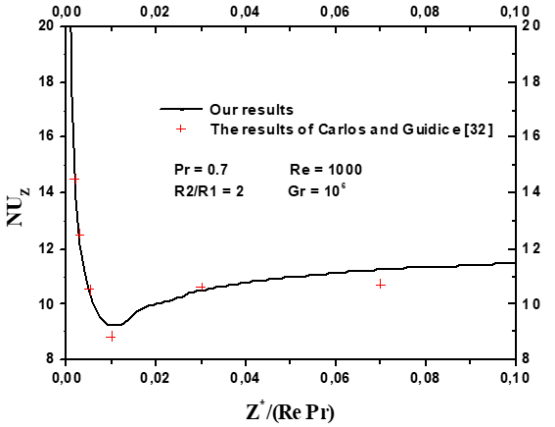

Fig. 2. Axial evolution of the averaged Nusselt number; a comparison with the results of Carlo and Guidice. [32]

A second validation of the numerical code used in this study is the comparison of our results with those of Nouar. [33] who studied numerically the conjugate mixed convection heat transfer in annular duct with the controlling parameters of the problem: L/D_h=125, Re=35, Pr=557.3 and Gr=6,000. In figure 3, we present the temperature variation at the top (θ=0) and at the bottom (θ=π) of the external interface of the annulus (external fluid-outer cylinder).

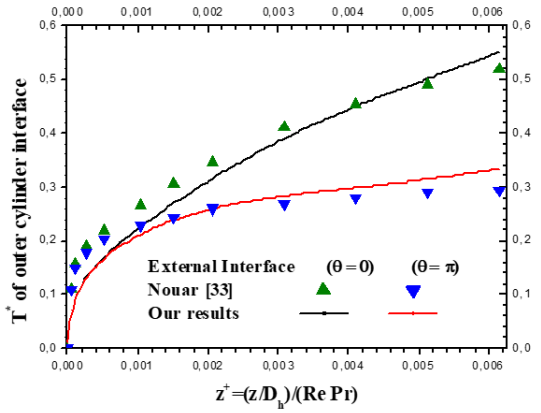

Fig. 3. Axial evolution of the interface temperature (external fluid-outer cylinder); a comparison with the results of Nouar. [33]

The temperature and the axial position are presented in dimensionless form in accordance with reference [33]; the axial position is normalized by the product (Re Pr). It is clear that our results are in good agreement with those of the cited reference.

4. Results and discussions

4.1 Development of hydrodynamic flow

All results presented in this paper were calculated for Reynolds number Re=399.02, Prandtl number Pr=8.082 and Grashof number (for mixed convection) Gr=12801, while the height of the fin is equal to 0.12 cm, which represents 25% of the hydraulic diameter.

In the case of the longitudinal fins, the hydrodynamic field is characterized by a main flow along the axial direction and a secondary flow influenced by the density variation with temperature, which occurs in the plane $(r^*-\theta)$. The transverse flow vectors are presented at the annulus exit in fig. 4 for 8 longitudinal fins placed at $\theta = \pi/8,\ 3\pi/8,\ 5\pi/8,\ 7\pi/8,\ 9\pi/8,\ 11\pi/8,\ 13\pi/8$ and $15\pi/8$. This transverse flow is explained as follows: the hot fluid moves along the inner wall of the external cylinder from the bottom (θ=π) to the top (θ=0), this movement is blocked by the walls of the longitudinal fins.

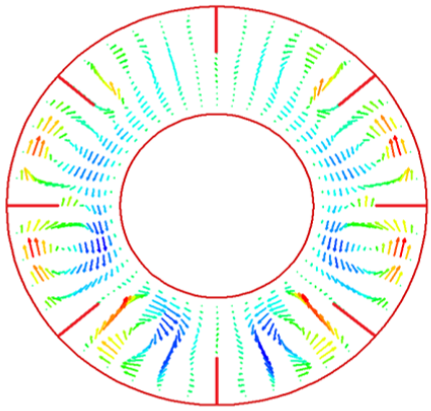

Fig. 4. Development of the secondary flow at the annulus exit

After, a portion of the fluid continues moving upwardly under the effect of the thermal buoyancy force while another part is conveyed downwardly with the relatively cold fluid which descends near of the inner cylinder. The transverse flow in the $(r^*-\theta)$ plane is represented by counter rotating cells; the cells number is proportional to longitudinal fins number used. The vertical plane passing through the angles $(\theta = 0)$ and $(\theta = \pi)$ is a plane of symmetry.

The position of maximum azimuthal velocity $V^*_{\theta\ max}$ in some axial positions is represented in table 1.

Table1 Maximum azimuthal velocity at some axial positions; Gr=12801

	$V^*_{\theta max}$	0.0046	0.0163	0.0171	0.0164	0.0169
Positions	z^*	11.549	55.027	83.560	163.72	217.39
	r^*	1.004	0.973	0.973	0.989	0.989
	θ	1.892	1.892	1.892	1.892	1.892

Regarding axial flow, this latter is axisymmetric in the forced convection case; at a given section, the axial velocity takes a minimum value (0) at the walls of pipes and fins and a maximum value between each two longitudinal fins, at the exit of the annulus $V^*_{z\ max}$ is equal to 1.658located at r^*=0.817 and θ =π/8, 3π/8, 5π/8, 7π/8, 9π/8, 11π/8, 13π/8, 15π/8.

In the mixed convection case (Gr=12801), the axial velocity is influenced by the generation of the secondary flow which causes an angular variation explained as follows: the thermal viscosity is inversely proportional to the fluid temperature and the axial velocity increases with the decrease of viscosity, automatically we will have an axial velocity relatively high in the upper part of the annulus where the fluid temperature is greater than that of the lower portion. In table 2, we present the position of the maximum axial velocity in some axial positions.

Table 2 Maximum axial velocity at some axial positions; Gr=12801

z^*	11.54	55.02	83.55	163.72	217.39
$V^*_{z\ max}$	1.671	1.690	1.787	2.040	2.031
r^*	0.801	0.833	0.817	0.770	0.754
θ	0.464	0.464	0.393	0.393	0.393

In fig. 5, we present an illustration of the variation of the axial velocity at the annulus exit (z^*=217.39) for both forced and mixed convection.

In the case of the transversal fins, the position of fins is only in selected axial sections at z^*=41.440, 84.918, 128.396, and 171.874. So the presentation of the results is based on the variation of the thermal and dynamic fields in the vicinity of the transverse fins. Far from these sections, the secondary motion is similar to that of simple annulus: the hot fluid moves upwards near the outer cylinder and the relatively cold fluid moves downwards near the inner cylinder.

The secondary flow vectors mapping around the first transversal fin section (z^*=41.440) is illustrated in fig. 6. At z^*=40.081 (just before the transverse fin), the vectors of the secondary flow near the hot wall change direction by creating a radial movement directed towards the internal cylinder allowing the fluid passes to z^*=41.440 between the internal cylinder and the fin. After passing through the transverse fin at z^*=42.799, the radial movement of the fluid is directed a second time toward the outer cylinder to return the fluid to the initial occupied state before the fin. From z^*=52.309, the vectors of the secondary flow discussed previously (annulus without fins) begin to reappear.

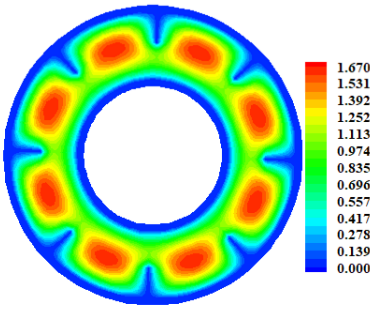

(a) Forced convection

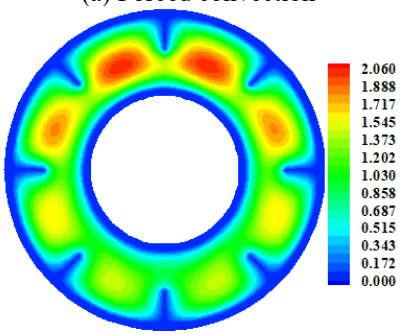

(b) Mixed convection (Gr=12801)

Fig. 5. Axial velocity profile at the annulus exit

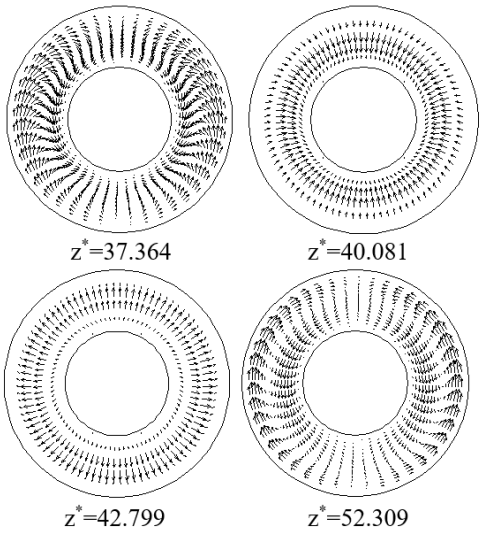

Fig. 6. Development of secondary flow around the first transverse fin

With regard to axial flow, far from the axial section of the transverse fin, the axial flow resembles that of an annulus without fins. However, just before the transverse fin, a radial movement of the fluid is created, this movement allowed to change the direction of the axial velocity facing the wall of the fin towards the inner cylinder so that it passes between the internal cylinder and the fin.

Thereafter, the radial movement of the fluid is directed towards the outer cylinder in order that the fluid returns to the initial state occupied before the fin.

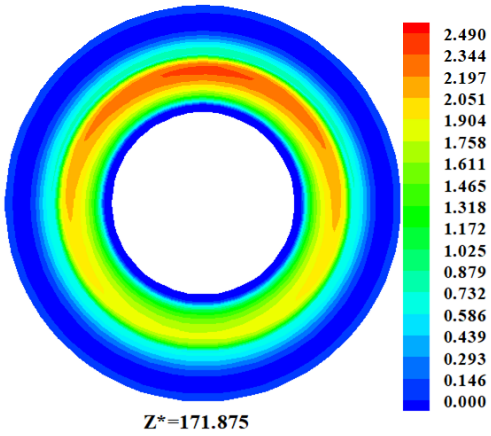

Fig. 7. Polar distribution of axial velocity at the fourth transverse fin; Gr=12801

The reduction in the passage section between the inner cylinder and each transverse fin results in a significant increase in the axial speed in this position. This sudden change in axial flow is repeated in every section of a transverse fin. The polar distribution of axial flow at the fourth transverse fin at z^*=171.875 is shown in fig.7.

4.2 Development of the thermal field

(1) The temperature field

In forced convection, the thermal field in the presence of eight longitudinal fins is axisymmetric. At a given section the isotherms of the fluid reach there minimum temperature on the wall of the inner cylinder,which then increases as it approaches the fins and the outer cylinder. At this temperature increases more and more near from the fins and the outer cylinder. At z^*=7.473, the maximum temperature of the fluid is equal to 0.09695 located at r^*=1.044 and θ=π/8, 3π/8, 5π/8, 7π/8, 9π/8, 11π/8, 13π/8 and 15π/8. This temperature increases to 0.1349, 0.2285, 0.3106 and 0.3807 in the axial positions z^*=14.266, $L^*/4$, $L^*/2$, $3L^*/4$ respectively. At the exit of the annulus, the temperature of the fluid reaches its absolute maximum which is equal to 0.4414, in this axial

position the temperature of each fin varies from 0.3892 to 0.4311. In the presence of volumetric heating, a transverse flow exists and thus changes the axisymmetric distribution of fluid and pipes wall temperature and gives it an angular variation. In this case the maximum temperature is always located at the top of solid-fluid interface of annulus at r^*=1.044 and θ=0 just at the right and the left of the vertical fin placed at θ=0, because the hot fluid is driven by the secondary motion towards the top of the annulus.

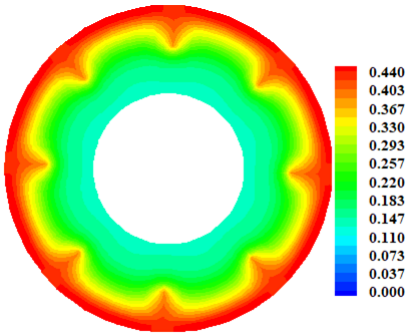

(a) Forced convection

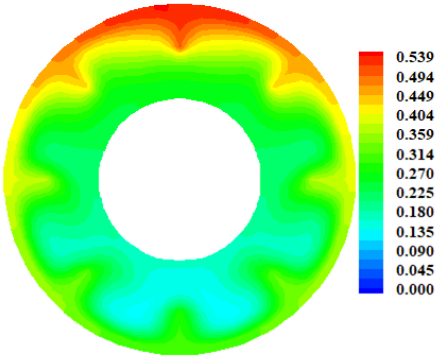

(b) Mixed convection (Gr= 12801)

Fig. 8. Axial temperature profile at the annulus exit

At z^*=11.549, the maximum temperature is equal to 0.1301, this temperature increases to 0.2569, 0.3204, 0.3728, 0.4651 and 0.5356 for $z^*=L^*/4$, 83.559, $L^*/2$, $3L^*/4$ and $z^*=L^*$ respectively. The minimum temperature of the fluid is at the lower part of annulus. At $z^*=L^*/4$, the position of the minimum temperature is located at r^*=0.551. This position moves to r^*=0.567, 0.5982, 0.6294 and r^*=0.645 for z^*=83.559, $L^*/2$, $3L^*/4$ and $z^*=L^*$, respectively.

In fig. 8 we present the variation of axial temperature profileat the exit of annulus (z^*=217.39) for both forced and mixed convection.

In fig. 9, we represent the variation of the axial temperature at the end of each fin at r^*=0.817.

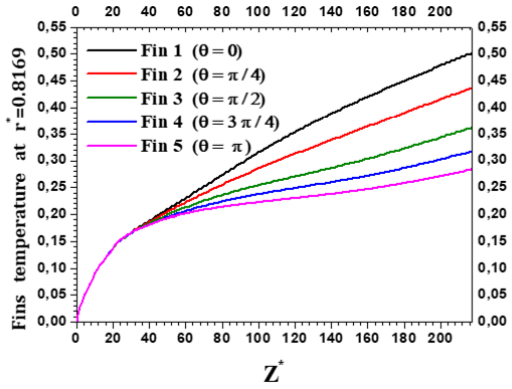

Fig. 9. Axial temperature variation of the fins at r^*=0.817

It is clear that the temperature of the vertical fin placed at θ=0is highest, followed by fin placed at θ=π/4, π/2, 3π/4 and π.

(2) Dimensionless heat flux at interfaces

The heat flow transferred to the fluid through the interface of the outer cylinder of the annulus in the case of mixed convection has an axial and azimuthal variation from the entrance to the exit; the vertical plane which passes through the axis of the cylinders is a plane of symmetry for this variation. At θ=0, π/4, π/2, 3π/4, π, 5π/4, 3π/2 and 7π/4, the cylindrical heat flow transferred to the fluid is zero because in these positions the outer cylinder is in contact with the longitudinal fins. Outside these azimuthal positions, at a given section the cylindrical heat flow takes a minimum value at the top of the cylinder and a maximum value at the bottom near from the fin located at θ=π because the hot fluid is always at the top while the relatively cold fluid is at the bottom. In fig. 10, the cylindrical heat flow is illustrated for the case of eight longitudinal fins. At the exit, the local heat flow from the external pipe takes a maximum value equal to 2.038 at θ=2.820. The heat flow released by the longitudinal fin placed at: (θ=0) is shown in fig. 11. The heat flow takes a maximum value equal to 4.039 at z^*=93.071 and r^*=0.817.

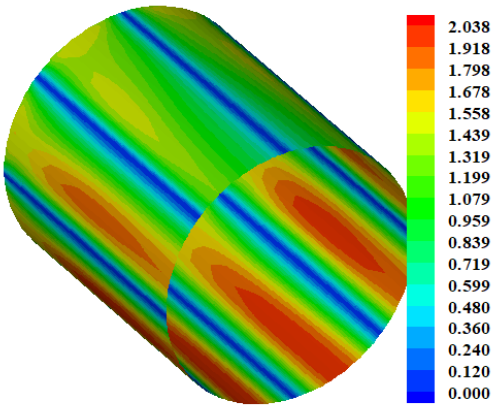

Fig. 10. Distribution of the local heat flow at the external cylinder interface for the case of longitudinal fins; Gr=12801

In the case of the transversal fins, the local heat flux at the cylindrical interface is shown in fig 12. It is clear that after each transverse fin the heat flux is relatively increased, this is due to the role of the transverse fins which serve to mix the fluid. So that the new fluid in the vicinity of the outer cylinder after the section of the transverse fin will have a lower temperature, this makes it possible to improve the heat transfer.

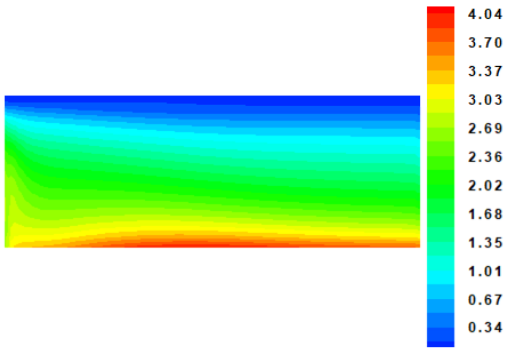

Fig. 11.Distribution of the local heat flow at the interface of the fin placed at (θ=0)

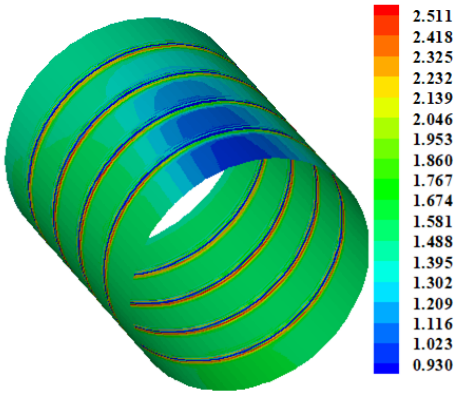

Fig. 12. Distribution of the local heat flow at the external cylinder interface for the case of transverse fins; Gr = 12801

The heat flux at the interface of the fourth transverse fin is shown in fig. 13.

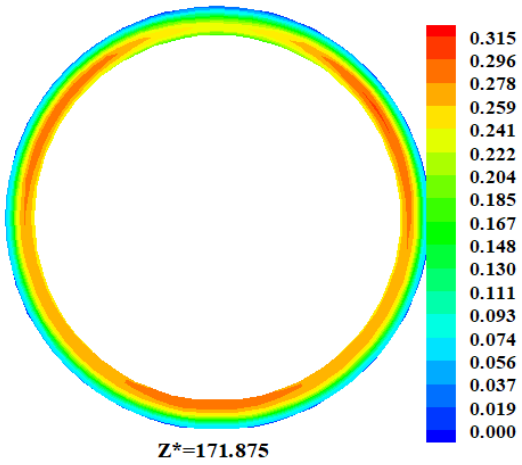

Fig. 13. Distribution of the local heat flow at the interface of the fin placed at (z^*=171.875)

The variation of the local heat flux at the fin interface follows a radial and angular variation such that it takes a maximum value equal to 0.315 located at r^*=1.004 and (θ=0.964 and θ=5.391).

(3) Evolution of the Nusselt number

The variation of the local Nusselt number at the interface of the external cylinder for the case of longitudinal fins is illustrated in fig 14. At the interface between the external cylinder and the fins, the local Nusselt number is observed to be zero. This phenomenon arises from the fact that

at this specific location, there is no heat flow towards the fluid.

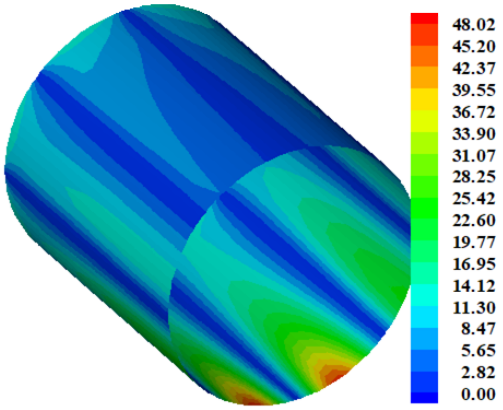

Fig. 14. Evaluation of the local Nusselt number at the external cylinder interface.

Beyond these specific azimuthal positions, the angular variation of the local Nusselt number reveals a minimum value at the top of the cylindrical interface and a maximum value at the bottom near the fin located at $\theta=\pi$. At the exit of annulus, the local Nusselt number takes a maximum value equal to 48.02 at θ=2.820.

The Nusselt number of the longitudinal fin placed at ($\theta=\pi$) is shown in fig. 15. The Nusselt number reaches a maximum value equal to 130.00 at z^*=217.39 and r^*=0.817.

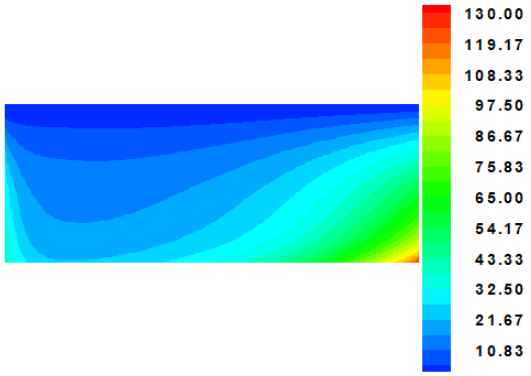

Fig. 15. Evaluation of the local Nusselt number at the longitudinal fin located at ($\theta=\pi$)

The comparison of the axial Nusselt numbers of the finned annulus is shown in fig.16. Quantitatively, there is a large increase in axial Nusselt when the number of fins is increased; this is due to the large increase in the exchange surfaces by adding the number of fins. At the exit of the annulus, the axial Nusselt number is equal to 22.887, 61.582 and 88.822 for the cases: two, four and eight longitudinal fins respectively. The average Nusselt numbers for these cases are: 18.99, 35.35 and 60.08.

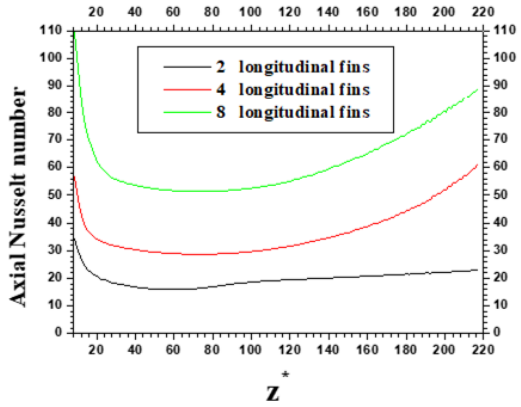

Fig. 16. Variation of the axial Nusselt number as a function of the number of longitudinal fins

Regarding the transversal fins, the local Nusselt number at the cylindrical interface of the outer cylinder is shown in fig. 17. Around the axial section of a transverse fin, the axial Nusselt variation is explained as follows: just before the transverse fin, Nu(z^*) decreases because in this section the movement of the fluid is directed towards the internal cylinder.

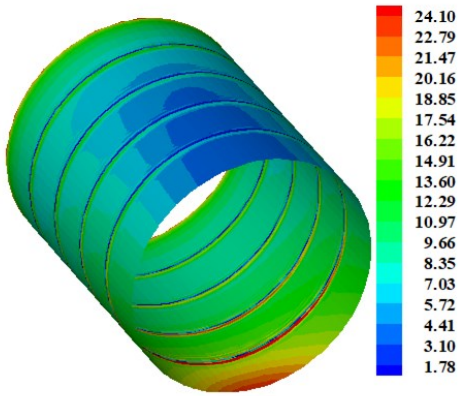

Fig. 17. Evaluation of the local Nusseltat the external cylinder interface

In the axial section of the transverse fin, Nu(z^*) increases considerably, then it decreases

a second time in the axial section following the transverse fin where the flow direction is once again redirected to the outer cylinder.

In fig.18, we present the local Nusselt number at the interface of the fourth transverse fin, this number follows a radial and angular variation such that it reaches a maximum value equal to 16.40 at r^*=0.895 and θ = π.

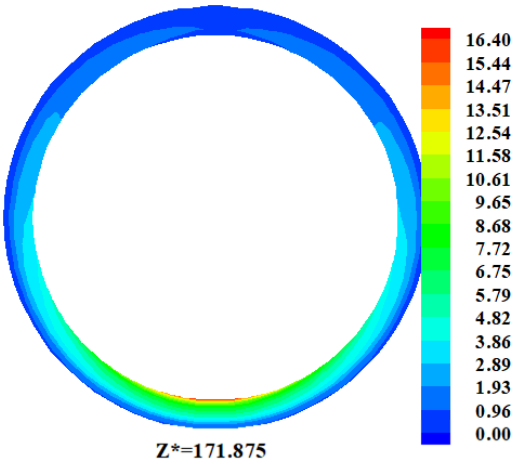

Fig. 18. Evaluation of the local Nusselt number at the transverse fin located at (z^*=171.875)

The axial Nusseltnumber variation for the case of transverse fins is compared with that of an annulus without fins in fig. 19.

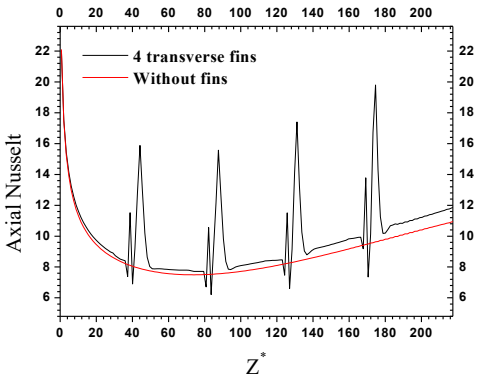

Fig. 19. Evaluation of the axial Nusseltnumber for the case of transverse fins; a comparison with the case without fins.

This comparison clearly shows that after each transverse fin there is an increase in the axial Nusselt compared to the case without fins, this is due on the one hand to the increase in the exchange surface by the fin itself, on the other hand to the role of the transverse fin which serves to mix the fluid well after each passage through these fins.

At the exit of the annulus, the axial Nusselt number is equal to 11.71, the mean Nusselt number for these case is: 10.40.

5. Conclusions

The results obtained from the work presented can be grouped into the following conclusions:

(1) Although the volumetric heat input in the solid thickness is constant, the heat flux at the solid-fluid interface is not constant: it varies with θ and z that is a characteristic of the considered mixed convection.

(2) The use of longitudinal fins increases the averageNusselt number compared to the case without fins with a rate of 109.83 %, 290.61% and 563.87% for the cases 2, 4 and 8 fins respectively.

(3) This improvement in the heat transfer is due to the important increase in the exchange surfaces by the use of the longitudinal fins.

(4) The obtained results clearly reveals that the heat flux released by the fins walls is greater than that released by the cylindrical surfaces; this is justified by the large value of the local Nusselt number of the fins.

(5) The use of four transverse fins increases the average Nusselt number compared to the case without fins with a rate of 14.92%. It is clear that this increase is less important than that of the longitudinal fins.

(6) The transverse fins participate in an indirect way in the improvement of heat transfer; their location facing the flow makes it possible to reorganize the structure of the flow for each passage through these fins, which serves to mix the fluid and increasing the heat transfer at cylindrical interfaces.

(7) The number of the fins is also important factor in improving heat transfer.

References

[1] S.V. Patankar, M. Ivanovic and E.M. Sparrow, “Analysis of turbulent flow and heat transfer in

internally finned tubes and Annuli", J. Heat Transfer, Vol. 101, pp. 29-37, (1979).

[2] A.K. Agrawal and S. Sengupta, "Laminar flow and heat transfer in a finned tube annulus", Int.J. Heat and Fluid Flow, Vol. 11(1), pp. 54-59, (1990).

[3] M.I. Farinas, A. Garonand K. Saint-Lous, "Study of heat transfer in a horizontal cylinder with fins", Revue Générale de Thermique, Vol. 36, pp. 398-410, (1997).

[4] Khemici. M, Boufendi. T and Touahri. S, "Numerical study of developing laminar mixed convection in a heated annular duct with temperature dependent properties", Thermal Science, Vol. 23, N°6A, pp. 3411-3423, (2019).

[5] Touahri. S, Boufendi. T, "Conjugate heat transfer with variable fluid properties in a heated horizontal annulus", Heat Transfer Research, Vol. 46, Issue 11, pp. 1019-1038, (2015).

[6] Touahri. S, Boufendi. T, "The 3D Computational Study of the heat transfer enhancement by using of the longitudinal and transversal internal fins in a heated horizontal pipe", Int. J. of Materials, Mechanics and Manufacturing, Vol. 4, No 4, pp. 282-287, (2016).

[7] Benhacine1. H, Mahfoud. B and Salmi. M, "Stability of conducting fluid flow between coaxial cylinders under thermal gradient and axial magnetic Field", Int. J. of Thermofluid Science and Technology, Vol. 9, Issue 2, Paper No. 090202, (2022).

[8] Liu. L, Te. S, Yang. C, Xiaolong. Y, Ling. Z, Ziyong. C, Lin. Z, Weigang. X, Shi. B, "Experimental and numerical investigation on the flow and heat transfer characteristics of the tube with an integrated internal longitudinal fin", Int. J. of Thermal Science, 183: 107857 (2023).

[9] Z. Yuzhu, L. Zhang, S. Bu, Cheng Sun, W. Xu, Y. Xiao and L. Liu, "Study on Heat Transfer characteristics of the Whole Plate Fin Tube Cooler", Int. J. of Thermofluid Science and Technology, Vol. 7 (2), Paper No. 070204, (2020).

[10] Gourari. S, Mebarek-Oudina. F, Hussein, A.K, Kolsi. L, Hassen. W and Younis. O, "Numerical study of natural convection between two coaxial inclined cylinders", International Journal of Heat and Technology, Vol. 37, No. 3, 2019 , pp. 779-786.

[11] Elkhazen. M, Hassen. W, Gannoun. R, Hussein. A.K, and Borjini. M, "Numerical study of electro convection in a dielectric layer between two cofocal elliptical cylinders subjected to unipolar injection", Journal of Engineering Physics and Thermophysics, Vol. 92, No. 5 , (2019) , pp. 1318-1329.

[12] Hussein. A.K, "Applications of nanotechnology in renewable energies-A comprehensive overview and understanding". Renew Sustain Energy Rev. (2015); 42: 460-476.

[13] Hussein. A.K, "Applications of nanotechnology to improve the performance of solar collectors-recent advances and overview". Renew Sustain Energy Rev. (2016); 62: 767-792.

[14] Hussein. A.K, Li. D, Kolsi. L, Kata. S, Sahoo. B, "A review of nanofluid role to improve the performance of the heat pipe solar collectors". Energy Proc. (2017); 109:417-424.

[15] Hussein. A.K, Walunj. A, and Lioua. K, "Applications of nanotechnology to enhance the performance of the direct absorption solar collectors", Journal of Thermal Engineering 2, No. 1 (2016): 529-540.

[16] Mahian. O, Kolsi. L, Amani. M, Estellé. P, Ahmadi. G, Kleinstreuer. C, Marshall. J, Siavashi. M, Taylor. R, Niazmand. H, Wongwises. S, Hayat. T, Kolanjiyil. A, Kasaeian . A, Pop I. Recent advances inmodeling and simulation of nanofluid flows-part I: fundamentals and theory. Phys Rep. (2019); 790:1-48.

[17] Mahian. O, Kolsi. L, Amani. M, Estellé. P, Ahmadi. G, Kleinstreuer. C, Marshall. J, Taylor. R, Abu-Nada. E, Rashidi. S, Niazmand. H, Wongwises. S, Hayat. T, Kasaeian. A, Pop I. Recent advances in modeling and simulation of nanofluid flows-part II: applications. Phys Rep. (2019); 791:1-59.

[18] Li. Z, Hussein. A.K, Younis. O, Afrand. M and Feng. S, "Natural convection and entropy generation of a nanofluid around a circular baffle inside an inclined square cavity under thermal radiation and magnetic field effects" , International Communications in Heat and Mass Transfer , Vol. 116 , Article No. 104650 , (2020).

[19] Ghachem. K, Hussein. A.K, Kolsi. L and Younis. O, "CNT–water nanofluid magneto-convective heat transfer in a cubical cavity equipped with perforated partition", The European Physical Journal Plus, Vol. 136: 377, (2021)

[20] Kamel. M.S, Ferenc.L and Kadhim. A.H, "Experimental studies of flow boiling heat transfer by using nanofluids." Journal of Thermal Analysis and Calorimetry 138, no. 6 (2019): 4019-4043.

[21] Benkhedda. M, Boufendi. T and Touahri. S, "Laminar mixed convective heat transfer enhancement by using Ag-TiO2-water hybrid Nanofluid in a heated horizontal annulus" Journal of Heat and Mass Transfer, Vol: 54, pp: 2799–2814 (2018).

[22] Tayebi. T, Chamkha. A.J, "Natural convection enhancement in an eccentric horizontal cylindrical annulus using hybrid nanofluids", Numer Heat Transf Part A Appl. (2017); 71:1159-1173.

[23] Tayebi. T, Chamkha. A.J, "Free convection enhancement in an annulus between horizontal confocal elliptical cylinders using hybrid nanofluids". Numer Heat Transf Part A Appl. (2016); 70:1141-1156.

[24] Tayebi. T, Chamkha. A. J, Öztop. H. F and Bouzeroura. L, "Local thermal non-equilibrium (LTNE) effects on thermal-free convection in a nanofluid-saturated horizontal elliptical non-Darcian porous annulus", Mathematics and Computers in Simulation (MATCOM), Elsevier, vol. 194(C), pages 124-140, (2022).

[25] Tayebi. T, Öztop. H.F, Chamkha. A.J, "MHD natural convection of a CNT-based nanofluid-filled annular circular enclosure with inner heat-generating solid cylinder". European Physical Journal Plus, Vol. 136: 150;(2021).

[26] Tayebi. T, Chamkha. A.J, "Analysis of the effects of local thermal non-equilibrium (LTNE) on thermo-natural convection in an elliptical annular space separated by a nanofluid-saturated porous sleeve". International Communications in Heat and Mass Transfer , Volume 129 (2), 105725, (2021).

[27] Al-Rashed. A, Aich. W, Kolsi. L, Mahian. O, Hussein. A.K and Borjini. M.N, "Effects of movable-baffle on heat transfer and entropy generation in a cavity saturated by CNT suspensions: three-dimensional modeling", Entropy, Vol. 19, 2017, pp: 200-216.

[28] Tayebi. T, Chamkha. A.J, Melaibari. A.A, Raouache. E, "Effect of internal heat generation or absorption on conjugate thermal-free convection of a suspension of hybrid nanofluid in a partitioned circular annulus", International Communications in Heat and Mass Transfer , Vol: 126 (4), 105397, (2021).

[29] H.D. Baehr and K. Stephan, "Heat and Mass Transfer", Springer- Verlag, Berlin, 1998.

[30] S.W. Churchill and H.S. Chu, "Correlating equation for laminar and turbulent free convection from a horizontal cylinder", Int. J. of Heat and Mass Transfer, Vol.18, pp. 1049-1053, (1975).

[31] S.V. Patankar, "Numerical Heat Transfer and Fluid Flow", McGraw-Hill, New-York, (1980).

[32] N. Carlo and S. D. Guidice, "Finite element analysis of laminar mixed convection in the entrance region of horizontal annular ducts", Numerical Heat Transfer, Part A, 29, pp. 313–330, (1996).

[33] C. Nouar, "Numerical solution for laminar mixed convection in a horizontal annular duct: temperature-dependent viscosity effect", Int. J. of Numerical Methods of Fluids, Vol. 29, pp. 849-864, (1999).